Nanoscale

ROYAL SOCIETY OF CHEMISTRY

COMMUNICATION

View Article Online
View Journal | View Issue

Cite this: *Nanoscale*, 2024, **16**, 9311

Received 6th February 2024,
Accepted 15th April 2024

DOI: 10.1039/d4nr00562g

rsc.li/nanoscale

Phase control of solid-solution RuIn nanoparticles and their catalytic properties†

Xin Zhou,[a] Megumi Mukoyoshi, *[a] Kohei Kusada, [a,b,c] Tomokazu Yamamoto,[d] Takaaki Toriyama,[d] Yasukazu Murakami[d,e] and Hiroshi Kitagawa *[a]

The properties of solids could be largely affected by their crystal structures. We achieved, for the first time, the phase control of solid-solution RuIn nanoparticles (NPs) from face-centred cubic (fcc) to hexagonal close-packed (hcp) crystal structures by hydrogen heat treatment. The effect of the crystal structure of RuIn alloy NPs on the catalytic performance in the hydrogen evolution reaction (HER) was also investigated. In the hcp RuIn NPs, enhanced HER catalytic performance was observed compared to the fcc RuIn NPs and monometallic Ru NPs. The intrinsic electronic structures of the NPs were investigated by valence-band X-ray photoelectron spectroscopy (VB-XPS). The d-band centre of hcp RuIn NPs obtained from VB-XPS was deeper than that of fcc RuIn NPs and monometallic Ru NPs, which is considered to enable the hcp RuIn NPs to exhibit enhanced HER catalytic performance.

The properties of metal nanomaterials are closely related to their crystal structures. For example, face-centred cubic (fcc) Ru nanoparticles (NPs) display better catalytic activities in CO oxidation than hexagonal close-packed (hcp) Ru NPs.[1] The low-frequency electrical noise of hcp Ag nanowires (NWs) is far less than that of conventional fcc Ag NWs.[2] The phase transition from cubic close packing (ccp) to the hcp crystal structure of Ru nanocrystals leads to the formation of a new RuC_x phase, which plays the role of an active site in accelerating the alkaline hydrogen evolution reaction (HER) kinetics.[3] Regarding metal alloy NPs with adjustable constituents and proportions, their properties can be significantly tuned by adjusting the crystal structure.[4–6] For instance, the face-centred tetragonal (fct) FePt NPs were found to be more stable than the fcc FePt NPs and could serve as an active catalyst for the oxygen reduction reaction.[7] The hcp PdRu NPs exhibit better oxygen evolution reaction (OER) performance than the fcc PdRu NPs.[8] Compared with fcc-$AuRu_3$ alloy NPs, hcp-$AuRu_3$ alloy NPs exhibit better thermal stability and durability in OER catalytic activity.[9] With different crystal structures, alloy NPs display different atomic arrangements and electronic structures on the surface, which affects the strength of surface–adsorbate interactions and thus leads to different catalytic properties.[10–12] Thus, controlling the crystal structure of alloy NPs holds promise for obtaining new functional materials. However, structure control of alloy NPs is difficult because once their constituents and proportions of elements are fixed, the thermodynamically most stable structure of the alloys is also determined.[13]

Platinum group metal (PGM) NPs have been extensively researched for their unique characteristics and high performance in catalysis.[14–16] Ru is one of the PGMs, and an hcp structure is the most stable phase for bulk Ru.[17] However, when the particles are of nanometre size, it is possible to obtain Ru NPs with an fcc crystal structure.[1] There have been studies on the properties of Ru nanocrystals with different crystalline phases and crystal sizes, and the different crystal structures of Ru nanocrystals exhibit different catalytic activities for many reactions, such as the reduction of *p*-nitrophenol by $NaBH_4$, the dehydrogenation of ammonia borane, the HER and the hydrogen oxidation reaction.[18–22] On the other hand, indium (In) is a non-precious metal which can also function as an efficient catalyst.[23] The Ru–In alloy system holds potential for further applications in catalysis. However, Ru and In are not miscible with each other even in the liquid phase at high temperatures,[24] which makes it a challenge to synthesise the alloy NPs. Recently, solid-solution RuIn alloy NPs with an fcc crystal structure have been obtained, and they are reported to exhibit

[a]*Division of Chemistry, Graduate School of Science, Kyoto University, Kitashirakawa-Oiwakecho, Sakyo-ku, Kyoto 606-8502, Japan.*
E-mail: mukoyoshi@ssc.kuchem.kyoto-u.ac.jp, kitagawa@kuchem.kyoto-u.ac.jp
[b]*The HAKUBI Center for Advanced Research, Kyoto University, Kitashirakawa-Oiwakecho, Sakyo-ku, Kyoto 606-8502, Japan*
[c]*JST-PRESTO, Honcho 4-1-8, Kawaguchi, Saitama 332-0012, Japan*
[d]*The Ultramicroscopy Research Center, Kyushu University, 744 Motooka, Nishi-ku, Fukuoka 819-0395, Japan*
[e]*Department of Applied Quantum Physics and Nuclear Engineering, Kyushu University, 744 Motooka, Nishi-ku, Fukuoka 819-0395, Japan*

†Electronic supplementary information (ESI) available: Experimental details, TEM images, STEM-EDX mapping, XPS spectra, and results of electrochemical measurements. See DOI: https://doi.org/10.1039/d4nr00562g

enhanced HER performance.[25] To date, no research has been reported on the effect of the crystal structure of RuIn solid-solution alloy NPs on catalytic properties due to the difficulties associated with controlling the crystal structure.

In this work, we achieved the phase control of solid-solution alloy NPs of Ru and In. The fcc RuIn NPs were transformed into hcp-structured RuIn NPs by heat treatment under a hydrogen (H_2) atmosphere. Powder X-ray diffraction (PXRD), scanning transmission electron microscopy (STEM) and the corresponding energy-dispersive X-ray spectroscopy (EDX) maps revealed that the synthesised RuIn NPs have a solid-solution fcc or hcp crystal structure. The variation of HER catalytic activity based on the crystal structure of the RuIn alloy NPs was also investigated. The hcp RuIn NPs exhibited higher catalytic performance than the fcc RuIn NPs and monometallic Ru NPs. From valence-band X-ray photoelectron spectroscopy (VB-XPS), it was revealed that the d-band centre of hcp RuIn NPs was deeper than that of fcc RuIn NPs and monometallic Ru NPs. This is considered to enable the hcp RuIn NPs to exhibit enhanced HER catalytic performance.

Fig. 1a shows the schematic illustration of the process to control the crystal structure of the RuIn solid-solution alloy NPs. According to our previous work, fcc RuIn NPs were obtained by wet chemistry and a cyclic voltammetry (CV) cleaning method.[25] The carbon-loaded fcc RuIn NPs were heated under a H_2 atmosphere to cause a phase transition from fcc to hcp. Experimental details are given in the ESI.†

Fig. 1b shows the PXRD patterns of the obtained NPs. Prior to the H_2 heat treatment, the synthesised RuIn NPs exhibited

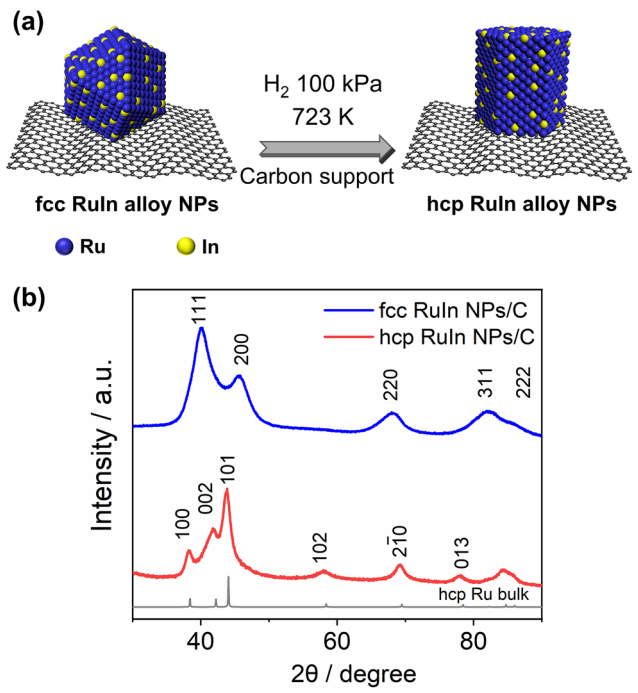

Fig. 1 (a) Schematic illustration of the process controlling the crystal structure of RuIn solid-solution alloy NPs. (b) PXRD patterns obtained from fcc and hcp RuIn NPs/C. Radiation wavelength: 1.5405(9) Å.

an fcc diffraction pattern. From the Rietveld refinement of the fcc RuIn NPs, the obtained lattice constant a was 3.8758(6) Å, which is larger than that of the calculated fcc lattice constant of Ru (a = 3.82 Å, by $\sqrt{2} \times a_{hcp}$) (Fig. S1†). The lattice constants a_{hcp} and c_{hcp} of the hcp Ru NPs determined from the Rietveld refinement were 2.7050(2) and 4.3054(4) Å, respectively (Fig. S2†). The increased lattice constant of the fcc RuIn NPs indicated the formation of alloy RuIn NPs. After the H_2 heat treatment, the RuIn NPs displayed an hcp diffraction pattern. The obtained lattice constants a_{hcp} and c_{hcp} of the hcp RuIn NPs from the Rietveld refinement were 2.7133(8) and 4.3388(4) Å, respectively (Fig. S3†), which are larger than those of monometallic hcp Ru NPs. Based on Vegard's law, the calculated composition ratios of Ru to In for the fcc and hcp RuIn alloy NPs were 0.938 : 0.062 and 0.948 : 0.052, respectively. X-ray fluorescence (XRF) results revealed that the atomic ratios of Ru to In in the fcc and hcp RuIn alloy NPs were 0.937 to 0.063 and 0.939 to 0.061, respectively, which is consistent with the PXRD results. These results indicated that the fcc and hcp RuIn NPs were successfully obtained. On the other hand, after heating at the same temperature (723 K) and for the same heating time (1.5 h) under vacuum conditions without H_2, the RuIn alloy NPs still contained the fcc phase (42%) with the hcp component (58%) (Fig. S4†), which implies that the phase transition was not fully complete. Meanwhile, the lattice parameters of both fcc and hcp components in vacuum-heat-treated RuIn NPs were also larger than those of fcc and hcp Ru NPs, indicating that both fcc and hcp components of the RuIn NPs form a solid-solution alloy structure. And the RuIn NPs were heated at different temperatures under an H_2 atmosphere for 1.5 h. According to the PXRD results, when the RuIn NPs were heated under an H_2 atmosphere at temperatures higher than 573 K, the phase transition from the fcc to hcp crystal structure occurred (Fig. S5†). It was assumed that heat treatment could induce a transition of the crystal structure from fcc to hcp in RuIn alloy NPs, which might be because the hcp crystal structure is a thermodynamically more favourable phase of RuIn alloy NPs. In addition, the RuIn alloy NPs are able to adsorb hydrogen, which accelerates atomic rearrangements to form different crystal structures.[26–28] It is well known that when metals absorb hydrogen molecules, hydrogen atoms could invade the lattice interstitials and generate defect structures, which promotes atomic diffusion and structure changes in alloys.[29–31] Therefore, the hydrogen heat treatment could accelerate the atomic rearrangements of fcc RuIn NPs to form the hcp crystal structure.

Atomic-resolution high-angle annular dark-field scanning transmission electron microscopy (HAADF-STEM) was carried out to further investigate the details of the atomic arrangement of the RuIn alloy NPs. The HAADF-STEM image of RuIn NPs in Fig. 2a and the corresponding fast Fourier transform (FFT) pattern (Fig. 2b) displayed an fcc nature. From the FFT pattern, the calculated d-spacings were estimated to be 1.9 and 1.4 Å for the $\{002\}_f$ (where f stands for fcc) and $\{022\}_f$ planes, respectively. An expanded STEM image with a lattice spacing of 1.9 Å further displayed a typical fcc atomic arrangement

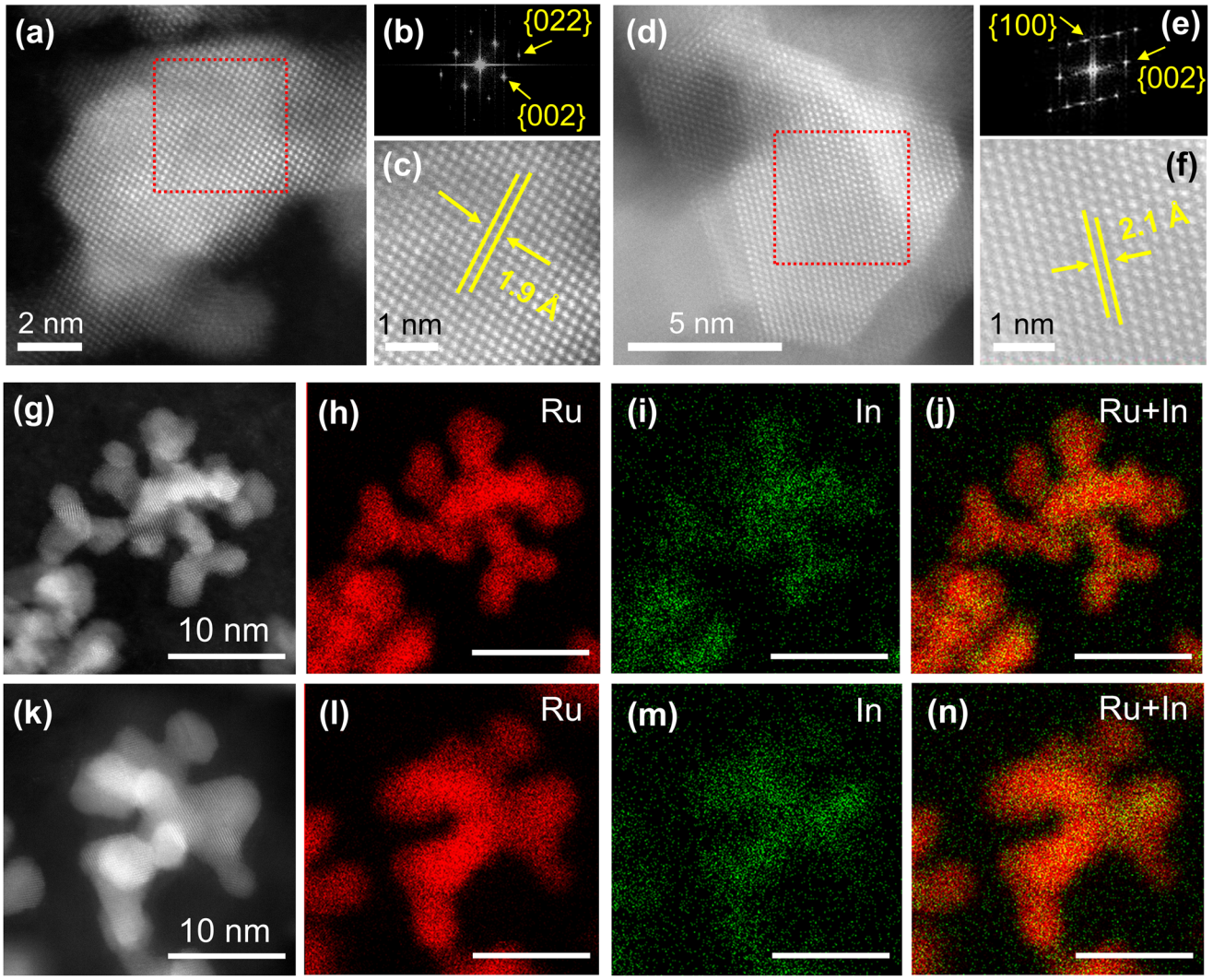

Fig. 2 (a) Atomic-resolution HAADF-STEM image obtained from the fcc RuIn NPs/C. (b) FFT pattern of (a). (c) An expanded view of the dashed red square region in (a). (d) Atomic-resolution HAADF-STEM image obtained from the hcp RuIn NPs/C. (e) FFT pattern of (d). (f) An expanded view of the dashed red square region in (d). (g) HAADF-STEM image, (h) Ru-L STEM-EDX map and (i) In-L STEM-EDX map of the fcc RuIn NPs/C. (j) The reconstructed overlay image of the maps shown in (h) and (i). (k) HAADF-STEM image, (l) Ru-L STEM-EDX map and (m) In-L STEM-EDX map of the hcp RuIn NPs/C. (n) The reconstructed overlay image of the maps shown in (l) and (m). Scale bar: 10 nm.

from the [100] zone axis (Fig. 2c). The STEM image and the FFT pattern of the RuIn NPs in Fig. 2d showed an hcp nature. According to the FFT pattern, the calculated *d*-spacings were estimated to be 2.3 and 2.1 Å for the $\{100\}_h$ (where h stands for hcp) and $\{002\}_h$ planes, respectively (Fig. 2e). An expanded STEM image shows a lattice spacing of 2.1 Å, which is a characteristic hcp atomic arrangement from the [010] zone axis (Fig. 2f). These observed lattice spacings were also in agreement with the structural information obtained from the Rietveld refinement. These results indicated the successful control of the crystal structure of RuIn alloy NPs. In addition, from HAADF-STEM images and the corresponding EDX maps, we confirmed that Ru and In elements are distributed randomly and homogeneously in both fcc and hcp RuIn alloy NPs, indicating the solid-solution alloy structures of both fcc and hcp RuIn alloy NPs (Fig. 2g–n). The particle size of the fcc and hcp RuIn NPs was calculated to be 5.0 ± 2.5 nm and 5.4 ± 2.6 nm, respectively, by transmission electron microscopy (TEM) (Fig. S6†). The estimated diameter of the NPs was averaged over 200 NPs.

X-ray photoelectron spectroscopy (XPS) was carried out to determine the oxidation state of the fcc RuIn NPs, hcp RuIn NPs and monometallic hcp Ru NPs. From the In 3d XPS spectra, two peaks were observed at binding energies (BEs) of 451.2 and 443.6 eV for fcc RuIn NPs and 451.0 and 443.4 eV for hcp RuIn NPs, respectively, which correspond to In $3d_{3/2}$ and In $3d_{5/2}$ of metallic In, respectively (Fig. S7†).[32,33] The Ru 3p spectra of fcc and hcp RuIn NPs each displayed two peaks at BEs of 461.7 and 483.9 eV and 461.6 and 483.9 eV, respectively, attributed to Ru $3p_{3/2}$ and Ru $3p_{1/2}$ of metallic Ru,

respectively (Fig. S8a and S8b†).[34] In comparison with the XPS results of monometallic Ru NPs (Fig. S8c†), a shift to lower BEs of the Ru 3p XPS peaks was observed in both fcc and hcp RuIn NPs. It is assumed that this is due to the electronic changes induced by the electron transfer from In to Ru in RuIn NPs.[35,36] The negligible difference in the XPS peak positions of fcc and hcp RuIn NPs is considered to be due to the similar homogeneous solid-solution structures of the alloy NPs in fcc and hcp crystal structures.[13] The XPS results further suggest that the solid-solution alloy RuIn NPs with an fcc or hcp structure was successfully formed.

We examined the HER catalytic performance of the carbon-loaded NPs in an Ar-saturated 0.5 M H_2SO_4 solution. The linear sweep voltammetry (LSV) curves (Fig. 3a) revealed that hcp RuIn NPs/C can achieve a current density of 10 mA cm^{-2} at an overpotential (η) of 28.5 mV, which shows a higher HER catalytic activity than commercial Pt NPs/C (35.3 mV), fcc RuIn NPs/C (35.5 mV) and hcp Ru NPs/C (53.7 mV) (Fig. 3b). As shown in Fig. 3c, the Tafel slope of hcp RuIn NPs/C (21.58 mV dec^{-1}) was found to be lower than that of commercial Pt NPs/C (22.02 mV dec^{-1}), fcc RuIn NPs/C (23.43 mV dec^{-1}) and hcp Ru NPs/C (37.08 mV dec^{-1}). The Tafel slope is an important indicator of the kinetic behaviour of the catalysts—the lower the value, the faster the reaction kinetics.[37] The Tafel slope for hcp RuIn NPs/C also showed that the rate-determining step of the HER is the Tafel step.[38] The hcp RuIn NPs/C also exhibited the highest mass activity (47.98 and 177.78 A g^{-1} for η_{10} and η_{20}, respectively), compared with commercial Pt NPs/C (24.48 and 83.02 A g^{-1} for η_{10} and η_{20}, respectively), fcc RuIn NPs/C (24.18 and 96.08 A g^{-1} for η_{10} and η_{20}, respectively) and hcp Ru NPs/C (15.48 and 38.08 A g^{-1} for η_{10} and η_{20}, respectively), as shown in Fig. 3d and S9.† The results suggest that hcp RuIn alloy NPs exhibit improved HER catalytic performance. Furthermore, chronoamperometry measurements for a durability test were performed on the NPs (Fig. S10 and S11†). No significant degradation of the LSV curves occurred after a 10 h durability test, indicating the durable catalytic stability of the hcp and fcc RuIn NPs. According to the XRF results, the atomic ratios of Ru to In in the fcc and hcp RuIn NPs after the chronoamperometry measurement were 0.948 to 0.052 and 0.947 to 0.053, respectively. The results showed that after the stability test, only a slight decrease in the In content was observed, with most of the In content remaining in the alloy NPs. XPS measurement was also carried out on the RuIn NPs after the stability measurement (Fig. S12†). The Ru 3p and In 3d XPS spectra of both fcc and hcp RuIn NPs after the stability test exhibited only XPS peaks attributed to the metallic Ru and In, suggesting that the Ru and In elements in the alloy NPs are still in the metallic state. The results showed that the composition and oxidation state of RuIn NPs did not change significantly before and after the chronoamperometry measurement.

Turnover frequency (TOF) is a possible descriptor of the intrinsic activity of an electrocatalyst.[39–41] The TOF values were determined based on the contribution of the electrochemically active surface area (ECSA), which was estimated by the copper underpotential deposition method (Cu UPD) (Fig. S13†). At an overpotential of 10 mV, the hcp RuIn NPs/C showed the highest TOF value of 0.81 H_2 s^{-1} among those of fcc RuIn alloy NPs/C (0.44 H_2 s^{-1}) and hcp Ru NPs/C (0.25 H_2 s^{-1}) (Fig. S14†). The above results indicate that hcp RuIn NPs show better HER catalytic performance than fcc RuIn NPs and monometallic hcp Ru NPs, which indicates that the catalytic properties of the alloy NPs are closely related to their crystal structure.

The atomic arrangement and electronic structure on the surface of the alloy NPs are different with different crystal structures. These variations in the geometry and electronic structure on the surface of the catalyst will affect the adsorption behaviour of metals and intermediates.[42–44] It is widely recognized that HER electrocatalysts with high performance should have a moderate binding strength between metal active sites and intermediate H*.[45,46] The concept of the d-band centre proposed by Nørskov *et al.* has been proved to be an effective indicator of the binding strength of the intermediates during the electrocatalytic HER.[47–49] VB-XPS was carried out to investigate the intrinsic electronic structure of the NPs. Fig. 4a and S15† show the VB-XPS spectra of the commercial Pt NPs/C, hcp RuIn NPs, fcc RuIn NPs and hcp Ru NPs. The d-band centre of the commercial Pt NPs/C calculated from the VB-XPS spectra is −4.04 eV. As calculated from the VB-XPS spectra, the d-band centre of hcp RuIn NPs is deeper (−3.96 eV) than that of fcc RuIn NPs (−3.92 eV) and hcp Ru NPs (−3.86 eV) (Fig. 4b). According to the density functional theory (DFT) calculations, the Ru of the hcp structure has a lower total energy in the valence band region than the fcc Ru.[50] The results indicated that hcp is the most stable phase of Ru. The different stable states among different structures are considered to result in a variation of the d-band centre. It is reported that the DFT calculations reveal that the metastable fct Au has an

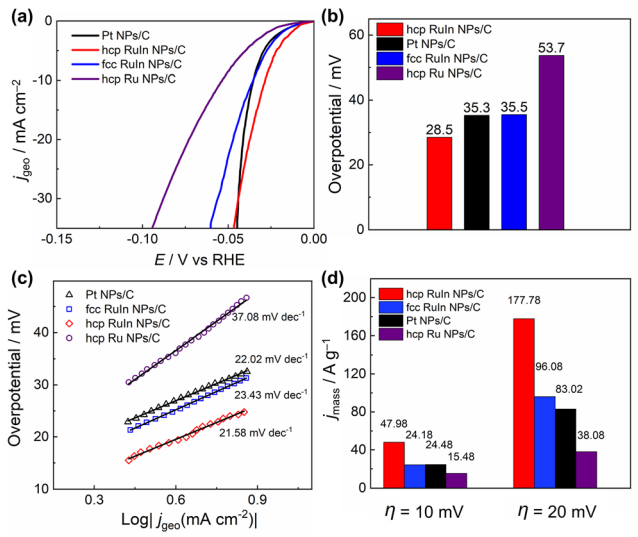

Fig. 3 HER catalytic activities of RuIn alloy catalysts. (a) LSV curves of commercial Pt NPs/C, fcc RuIn NPs/C, hcp RuIn NPs/C and hcp Ru NPs/C. (b) Overpotentials of the catalysts at a current density of 10 mA cm^{-2}. (c) Tafel slopes for the catalysts. (d) Mass activities of the catalysts at 10 mV and 20 mV overpotentials.

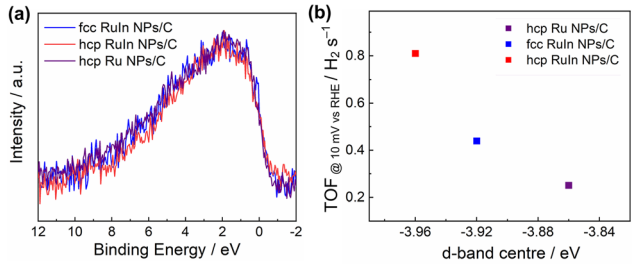

Fig. 4 (a) VB-XPS spectra obtained from hcp Ru NPs/C, hcp RuIn NPs/C and fcc RuIn NPs/C and (b) d-band centres of hcp Ru NPs/C, hcp RuIn NPs/C and fcc RuIn NPs/C calculated from the VB-XPS spectra.

upshifted d-band centre compared to the stable fcc Au.[51] Therefore, the hcp RuIn NPs show a downshifted d-band center compared to the fcc RuIn NPs. According to the d-band theory, a deeper d-band centre implies weaker adsorption and better desorption of intermediate H*.[52] The d-band centre of the hcp RuIn NPs is downshifted compared with that of the fcc RuIn NPs and hcp Ru NPs, suggesting that the adsorption of the metal to intermediate H* is weakened, thus resulting in enhanced HER performance of the hcp RuIn NPs.

In addition, metals with fcc or hcp crystal structures have different crystal morphologies. It is well-known that NPs with different crystal structures will expose different crystalline facets, and according to the first-principles calculations, the fcc Ru exposes mainly the {111} and {110} crystal facets and the hcp Ru exposes mainly the $\{10\bar{1}\bar{1}\}$, {0001} and $\{10\bar{1}\bar{0}\}$ crystal facets.[53] Furthermore, due to the heat treatment, the hcp RuIn NPs could selectively expose the stable facets with different adsorption and dissociation behaviors in catalytic reactions. Therefore, the catalytic properties of the alloy NPs could be controlled by their crystal structure. In this study, the HER performance of RuIn alloy NPs with an hcp structure is higher than that of the alloy NPs with an fcc structure.

Conclusions

In summary, for the first time, we achieved the phase control of solid-solution RuIn NPs from fcc to hcp crystal structures by H_2 heat treatment. PXRD, STEM and the corresponding EDX maps revealed that the obtained RuIn NPs have a solid-solution fcc or hcp crystal structure. The effect of the crystal structure of the alloy NPs on HER catalytic performance was also investigated. The hcp RuIn NPs exhibited better HER catalytic performance than the fcc RuIn NPs and monometallic Ru NPs. VB-XPS analysis showed a deeper d-band centre of hcp RuIn NPs compared to that of fcc RuIn NPs and monometallic Ru NPs, which is considered to result in the improved HER catalytic performance of hcp RuIn NPs. This study provides an insightful concept for obtaining efficient catalysts through phase control. Furthermore, such a concept is not only applicable to binary alloy systems but can also be extended to multi-constituent systems.

Author contributions

X. Z., M. M., K. K., and H. K. conceptualized the work and designed the experiments; X. Z. synthesised the materials; T. Y., T. T., and Y. M. carried out the STEM characterization; X. Z. and M. M. wrote the manuscript; all authors contributed to the discussion of results and approved the final version of the manuscript.

Conflicts of interest

There are no conflicts to declare.

Acknowledgements

We acknowledge the support from a Grant-in-Aid for Research Activity Start-up No. 22K20557 and a Grant-in-Aid for Specially Promoted Research No. 20H05623. This work was also supported by FY 2022 Kusunoki 125 of the Kyoto University 125th Anniversary Fund. STEM analyses were supported by "Advanced Research Infrastructure for Materials and Nanotechnology in Japan (ARIM)" of the Ministry of Education, Culture, Sports, Science and Technology (MEXT) under proposal No. JPMXP1223KU0008 and JPMXP1223KU0009.

References

1 K. Kusada, H. Kobayashi, T. Yamamoto, S. Matsumura, N. Sumi, K. Sato, K. Nagaoka, Y. Kubota and H. Kitagawa, *J. Am. Chem. Soc.*, 2013, **135**(15), 5493–5496.
2 A. Singh, T. P. Sai and A. Ghosh, *Appl. Phys. Lett.*, 2008, **93**(10), 102107.
3 J. Kim, H. J. Kim, B. Ruqia, M. J. Kim, Y. J. Jang, T. H. Jo, H. Baik, H. S. Oh, H. S. Chung, K. Baek, S. Noh, M. Jung, K. J. Kim, H. K. Lim, Y. S. Youn and S. I. Choi, *Adv. Mater.*, 2021, **33**(48), 2105248.
4 K. Kusada and H. Kitagawa, *Adv. Mater.*, 2016, **28**(6), 1129–1142.
5 W. Zhan, J. Wang, H. Wang, J. Zhang, X. Liu, P. Zhang, M. Chi, Y. Guo, Y. Guo, G. Lu, S. Sun, S. Dai and H. Zhu, *J. Am. Chem. Soc.*, 2017, **139**(26), 8846–8854.
6 C. Wang, H. Yang, Y. Zhang and Q. Wang, *Angew. Chem., Int. Ed.*, 2019, **58**(18), 6099–6103.
7 J. Kim, Y. Lee and S. Sun, *J. Am. Chem. Soc.*, 2010, **132**(14), 4996–4997.
8 D. Wu, K. Kusada, S. M. Aspera, H. Nakanishi, Y. Chen, O. Seo, C. Song, J. Kim, S. Hiroi, O. Sakata, T. Yamamoto, S. Matsumura, Y. Nanba, M. Koyama, N. Ogiwara, S. Kawaguchi, Y. Kubota and H. Kitagawa, *ACS Mater. Au*, 2021, **2**(2), 110–116.
9 Q. Zhang, K. Kusada, D. Wu, S. Kawaguchi, Y. Kubota and H. Kitagawa, *Chem. Lett.*, 2018, **47**(4), 559–561.

10 S. L. A. Bueno, X. Zhan, J. Wolfe, K. Chatterjee and S. E. Skrabalak, *ACS Appl. Mater. Interfaces*, 2021, **13**(44), 51876–51885.
11 V. Petkov, B. Prasai, S. Shastri, J. W. Kim, S. Shan, H. R. Kareem, J. Luo and C. J. Zhong, *J. Phys. Chem. C*, 2017, **121**(14), 7854–7866.
12 S. Zeng, S. Shan, A. Lu, S. Wang, D. T. Caracciolo, R. J. Robinson, G. Shang, L. Xue, Y. Zhao, A. Zhang, Y. Liu, S. Liu, Z. Liu, F. Bai, J. Wu, H. Wang and C. J. Zhong, *Catal. Sci. Technol.*, 2021, **11**(17), 5712–5733.
13 Q. Zhang, K. Kusada, D. Wu, T. Yamamoto, T. Toriyama, S. Matsumura, S. Kawaguchi, Y. Kubota and H. Kitagawa, *J. Am. Chem. Soc.*, 2022, **144**(9), 4224–4232.
14 D. Wu, K. Kusada, T. Yamamoto, T. Toriyama, S. Matsumura, S. Kawaguchi and H. Kitagawa, *J. Am. Chem. Soc.*, 2020, **142**(32), 13833–13838.
15 A. T. Bell, *Science*, 2003, **299**(5613), 1688–1691.
16 S. N. Rashkeev, D. M. Ginosar, L. M. Petkovic and H. H. Farrell, *Catal. Today*, 2009, **139**(4), 291–298.
17 S. Okazoe, K. Kusada, D. Wu, T. Yamamoto, T. Toriyama, S. Matsumura, S. Kawaguchi, Y. Kubota and H. Kitagawa, *Chem. Commun.*, 2020, **56**(92), 14475–14478.
18 M. Zhao and Y. Xia, *Nat. Rev. Mater.*, 2020, **5**(6), 440–459.
19 S. H. Joo, J. Y. Park, J. R. Renzas, D. R. Butcher, W. Huang and G. A. Somorjai, *Nano Lett.*, 2010, **10**(7), 2709–2713.
20 H. Ye, Q. Wang, M. Catalano, N. Lu, J. Vermeylen, M. J. Kim, Y. Liu, Y. Sun and X. Xia, *Nano Lett.*, 2016, **16**(4), 2812–2817.
21 L. Li, C. Liu, S. Liu, J. Wang, J. Han, T. S. Chan, Y. Li, Z. Hu, Q. Shao, Q. Zhang and X. Huang, *ACS Nano*, 2022, **16**(9), 14885–14894.
22 Z. Wang and H. Wang, *ACS Appl. Mater. Interfaces*, 2023, **15**(30), 36676–36687.
23 W. Guo, X. Tan, J. Bi, L. Xu, D. Yang, C. Chen, Q. Zhu, J. Ma, A. Tayal, J. Ma, Y. Huang, X. Sun, S. Liu and B. Han, *J. Am. Chem. Soc.*, 2021, **143**(18), 6877–6885.
24 H. Okamoto, *Bull. Alloy Phase Diagrams*, 1988, **9**, 704–704.
25 X. Zhou, M. Mukoyoshi, K. Kusada, T. Yamamoto, T. Toriyama, Y. Murakami, T. Ina, S. Kawaguchi, Y. Kubota and H. Kitagawa, *ACS Mater. Lett.*, 2024, **6**, 353–359.
26 T. Si, Y. Cao, Q. Zhang, D. Sun, L. Ouyang and M. Zhu, *J. Mater. Chem. A*, 2015, **3**(16), 8581–8589.
27 K. Kusada, H. Kobayashi, R. Ikeda, Y. Kubota, M. Takata, S. Toh, T. Yamamoto, S. Matsumura, N. Sumi, K. Sato, K. Nagaoka and H. Kitagawa, *J. Am. Chem. Soc.*, 2014, **136**(5), 1864–1871.
28 G. Zepon, D. R. Leiva, R. B. Strozi, A. Bedoch, S. J. A. Figueroa, T. T. Ishikawa and W. J. Botta, *Int. J. Hydrogen Energy*, 2018, **43**(3), 1702–1708.
29 K. Kusada, H. Kobayashi, R. Ikeda, Y. Kubota, M. Takata, S. Toh, T. Yamamoto, S. Matsumura, N. Sumi, K. Sato, K. Nagaoka and H. Kitagawa, *J. Am. Chem. Soc.*, 2014, **136**(5), 1864–1871.
30 N. Chandrasekhar and D. S. Sholl, *J. Alloys Compd.*, 2014, **609**, 244–252.
31 H. Kohlmann, G. Renaudin, K. Yvon, C. Wannek and B. Harbrecht, *J. Solid State Chem.*, 2005, **178**(4), 1292–1300.
32 S. Cingarapu, M. A. Ikenberry, D. B. Hamal, C. M. Sorensen, K. Hohn and K. J. Klabunde, *Langmuir*, 2012, **28**(7), 3569–3575.
33 E. Laine, M. Tamminen, R. Mäkelä and M. Pessa, *J. Mater. Sci.*, 1983, **18**, 295–298.
34 N. Chakroune, G. Viau, S. Ammar, L. Poul, D. Veautier, M. M. Chehimi, C. Mangeney, F. Villain and F. Fiévet, *Langmuir*, 2005, **21**(15), 6788–6796.
35 Z. Jiang, W. Zhang, L. Jin, X. Yang, F. Xu, J. Zhu and W. Huang, *J. Phys. Chem. C*, 2007, **111**(33), 12434–12439.
36 E. Choi, S. J. Oh and M. Choi, *Phys. Rev. B: Condens. Matter Mater. Phys.*, 1991, **43**(8), 6360.
37 H. C. Li, P. C. Ji, Y. Teng, H. L. Jia and M. Y. Guan, *New J. Chem.*, 2023, **47**(20), 9628–9634.
38 Z. Yu, C. Wang, S. Guo, H. Yao, Z. Liang, R. Liu, K. Shi, C. Li and S. Ma, *Electrochim. Acta*, 2022, **403**, 139683.
39 D. Liu, G. Xu, H. Yang, H. Wang and B. Y. Xia, *Adv. Funct. Mater.*, 2023, **33**(7), 2208358.
40 H. J. Kim, E. Hong, Y. Hong, J. Kim, M. K. Kabiraz, Y. M. Kim, H. Lee, W. S. Seo and S. I. Choi, *Nanoscale*, 2023, **15**(12), 5816–5824.
41 S. Anantharaj, P. E. Karthik and S. Noda, *Angew. Chem., Int. Ed.*, 2021, **60**(43), 23051–23067.
42 A. Nilsson, L. G. M. Pettersson, B. Hammer, T. Bligaard, C. H. Christensen and J. K. Nørskov, *Catal. Lett.*, 2005, **100**, 111–114.
43 V. R. Stamenkovic, B. Fowler, B. S. Mun, G. Wang, P. N. Ross, C. A. Lucas and N. M. Markovic, *Science*, 2007, **315**(5811), 493–497.
44 J. K. Nørskov, T. Bligaard, B. Hvolbæk, F. Abild-Pedersen, I. Chorkendorff and C. H. Christensen, *Chem. Soc. Rev.*, 2008, **37**(10), 2163–2171.
45 S. Pan, C. Chang and Z. Yang, *Int. J. Hydrogen Energy*, 2023, **48**, 38655–38663.
46 B. Wang, F. Yang and L. Feng, *Small*, 2023, **19**(45), 2302866.
47 J. Greeley and J. K. Nørskov, *Surf. Sci.*, 2005, **592**(1–3), 104–111.
48 J. K. Nørskov, F. Abild-Pedersen, F. Studt and T. Bligaard, *Proc. Natl. Acad. Sci. U. S. A.*, 2011, **108**(3), 937–943.
49 B. Hammer, Y. Morikawa and J. K. Nørskov, *Phys. Rev. Lett.*, 1996, **76**(12), 2141.
50 S. Watanabe, T. Komine, T. Kai and K. Shiiki, *J. Magn. Magn. Mater.*, 2000, **220**(2–3), 277–284.
51 D. Yu, L. Gao, T. Sun, J. Guo, Y. Yuan, J. Zhang, M. Li, X. Li, M. Liu, C. Ma, Q. Liu, A. Pan, J. Yang and H. Huang, *Nano Lett.*, 2021, **21**(2), 1003–1010.
52 S. Shen, Z. Wang, Z. Lin, K. Song, Q. Zhang, F. Meng, L. Gu and W. Zhong, *Adv. Mater.*, 2022, **34**(13), 2110631.
53 H. Lin, J. X. Liu, H. Fan and W. X. Li, *J. Phys. Chem. C*, 2020, **124**(20), 11005–11014.

